JBIC Journal of Biological Inorganic Chemistry (2021) 26:881–893
https://doi.org/10.1007/s00775-021-01899-z

ORIGINAL PAPER

Co(II) complexes of curcumin and a ferrocene-based curcuminoid: a study on photo-induced antitumor activity

Dhananjay Das[1] · Aisha Noor[2] · Md Kausar Raza[3] · Tridib K. Goswami[1]

Received: 2 April 2021 / Accepted: 29 August 2021 / Published online: 22 September 2021

Abstract

Co(II) complexes having a ferrocene-based curcuminoid (Fc-curH) ligand viz. $[Co(L)_2(Fc\text{-}cur)]ClO_4$ (**1**, **2**), where L is phenanthroline base, namely, 1,10-phenanthroline (phen in **1**) and dipyrido[3,2-a:2',3'-c]phenazine (dppz in **2**) have been synthesized, characterized and evaluated as photochemotherapeutic agents in vitro. The corresponding Co(II) complexes of the naturally occurring polyphenol curcumin (curH), namely, $[Co(L)_2(cur)]ClO_4$ (**3**, **4**), where L is phen (in **3**) and dppz (in **4**) were synthesized and their photo-induced anticancer activities compared with their ferrocene containing counterparts **1** and **2**. The Co(II) acetylacetonato complex viz. $[Co(phen)_2(acac)]ClO_4$ (**5**) was structurally characterized through X-ray crystallography and used as control for cellular experiments. The Co(II) complexes having ferrocene-based curcuminoid are remarkably stable at physiological condition with higher lipophilicity compared to their curcumin analogues. The complexes display significant binding propensity to calf thymus (ct) DNA and human serum albumin (HSA). The complexes **1**–**4** display remarkable visible light induced cytotoxicity with the ferrocenyl analogues showing more phototoxic index (PI). The Co(II) curcumin complexes localize in the nucleus and mitochondria of A549 cells. The primary cell death mechanism is believed to be apoptotic in nature induced by light assisted generation of reactive oxygen species (ROS).

Graphic abstract

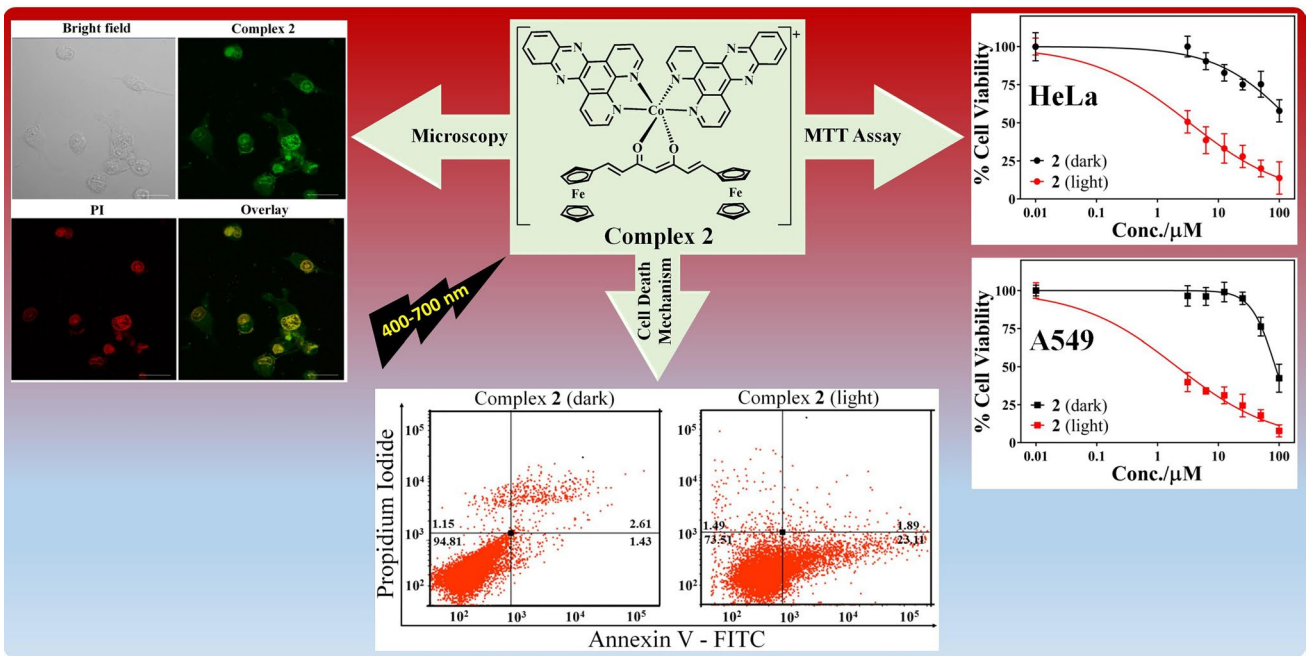

Extended author information available on the last page of the article

Keywords Co(II) complexes · Crystal structure · Curcumin · Ferrocene-based curcuminoid · Photo-induced cytotoxicity · ROS generation · Apoptosis

Introduction

The anticancer drug *cis*-diamminedichloroplatinum (II) (cisplatin) and other platinum analogues, such as carboplatin, oxaliplatin etc., are used successfully for the treatment of various cancers [1, 2]. The primary mechanism of action of these complexes is to interact with DNA via covalent linkages that inhibits vital cellular processes, such as replication and transcription resulting in cell death [3]. Despite their enormous use in cancer treatment, these drugs display various undesirable side effects, such as cardiotoxicity, nephrotoxicity, neurotoxicity and ototoxicity [4]. Inherent/acquired resistance developed by tumours and dose-limiting side effects are also major concerns [5]. This prompted search for alternate treatment regime for cancer that work more efficiently with lesser side effects. Use of light to activate a drug that is otherwise inactive is one of the most promising tools in this direction. Photodynamic therapy (PDT) is a prominent minimally invasive clinical treatment modality for cancer along with bacterial, fungal, viral infections and other skin ailments. PDT involves a photosensitizer (drug) along with molecular oxygen and light of suitable wavelength that can activate the photosensitizer to generate cytotoxic reactive oxygen species (ROS) [6, 7]. A few porphyrin-based PDT drugs, such as photofrin, Chlorin e6, Visudyne and Foscan, are clinically used in different countries [8, 9]. However, several disadvantages including prolonged cutaneous photo-sensitivity limit the use of these porphyrinic drugs [10, 11]. In recent years, a number of transition metal complexes have been designed and tested for their photochemotherapeutic potential against various tumor types using a wider range of exciting wavelengths [12–20].

Bioorganometallic chemistry has been rapidly evolving for designing molecules with very promising biomedical application, anticancer agents in particular [21–28]. Various metallocene's and metal-arene compounds are successfully screened for anticancer applications with some of them entering clinical trials [21, 22]. The ferrocene-analogue of breast cancer drug tamoxifen has been found to be effective against both hormone-dependent (ER +) and hormone-independent (ER-) breast cancer cells [23, 24]. A number of heavier transition metals, such as ruthenium, osmium, rhodium and iridium organometallic anticancer compounds, have shown promises in vitro [25–28].

Curcumin [1,7-bis(4-hydroxy-3-methoxyphenyl)-1,6-heptadiene-3,5-dione], a dietary spice for centuries in Asian countries, is a polyphenolic yellow pigment isolated from *Curcuma longa*. Although, curcumin has shown various pharmacological activities, such as anti-inflammatory, antimicrobial, anti-oxidant and anticancer properties, due to its rapid physiological degradation and poor absorption in tissues make its bioavailability extremely difficult [29, 30]. Various covalent modifications and coordination of the central β-diketonate moiety of the molecule to various metals are done extensively to improve its bioavailability [31–37]. We are interested in exploring the light-induced anticancer potential of transition metal complexes of curcumin analogues, i.e., curcuminoids that are easy to synthesize and much more stable than the natural polyphenol under physiological condition [38].

The present work stems from our continued interest to design and develop synthetic metallo-curcuminoinds with excellent photochemotherapeutic activities. Herein, we have synthesized a few Co(II) complexes having a ferrocene-appended curcuminoid (Fc-curH) along with phenanthroline bases, namely, $[Co(Phen)_2(Fc\text{-}cur)]ClO_4$ (**1**) and $[Co(dppz)_2(Fc\text{-}cur)]ClO_4$ (**2**), where phen is 1,10-phenonthroline, dppz is dipyrido[3,2-*a*:2′,3′-*c*]phenazine; Fc-curH is (1*E*,6*E*)-1,7-diferrocenyl-1,6-heptadien-3,5-dione and evaluated their anticancer activities in visible light (Scheme 1). The photochemotherapeutic potential of the Co(II) ferrocenyl-curcumin complexes are compared to activities of the corresponding Co(II) curcumin complexes, viz. $[Co(phen)_2(cur)]ClO_4$ (**3**) and $[Co(dppz)_2(cur)]ClO_4$ (**4**), to evaluate the role of the ferrocene-appended curcuminoid as anticancer agents. $[Co(phen)_2(acac)]ClO_4$ (**5**), where acacH is acetylacetone, was structurally characterized by X-ray crystallography and used as controls for various cellular experiments. The binding affinity of the complexes to calf thymus (*ct*) DNA and human serum albumin (HSA) were evaluated. The photochemotherapeutic potential of the complexes was assessed in vitro in HeLa and A549 cancer cell lines. The ability of the complexes to induce ROS was determined using DCFDA assay. Annexin-V-FITC-PI assay was employed to detect the ability of the complexes induce apoptotic cell death in A549 cells.

Experimental section

Materials and measurements

All chemicals and reagents of high quality were purchased from Sigma-Aldrich, Merck, Loba Chemie, SD Fine Chemicals and used as received. Calf thymus (ct) DNA, human serum albumin (HSA), fetal bovine serum (FBS), Dulbecco's phosphate buffered saline (DPBS), Dulbecco's Modified Eagle's Medium (DMEM),

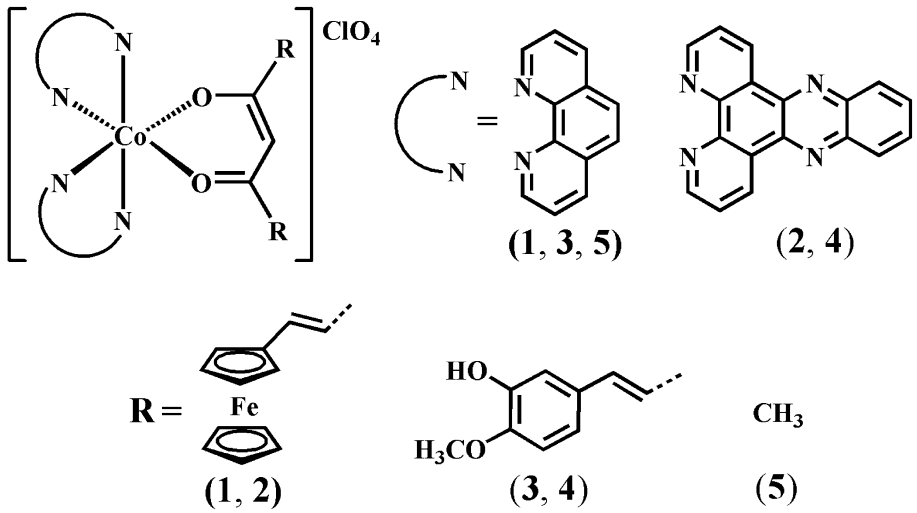

Scheme 1 Schematic drawings of the complexes $[Co(L)_2(Fc\text{-}cur)]ClO_4$ (**1**, **2**), $[Co(L)_2(cur)]ClO_4$ (**3**, **4**) and $[Co(L)_2(acac)]ClO_4$ (**5**) (L = phen in **1**, **3** and **5**; dppz in **2** and **4**)

3-(4,5-dimethylthiazol-2-yl)-2,5-diphenyltetrazolium bromide) (MTT), 2′,7′-dichlorofluorescein diacetate (DCFDA), propidium iodide (PI), and Annexin V-FITC were purchased from Sigma-Aldrich. The ligands (1*E*,6*E*)-1,7-diferrocenyl-1,6-heptadien-3,5-dione (Fc-curH) and dipyrido[3,2-*a*:2′,3′-*c*] phenazine (dppz) were prepared following reported literature [39, 40].

Elemental analysis (C, H and N) were performed on Thermo Finnigan Flash EA 1112 CHN analyzer. Infrared (IR) Spectra were recorded on Bruker ALPHA II compact FT-IR spectrometer using KBr pellets in the frequency range of 400–4000 cm^{-1}. Shimadzu UV-1800 and Hitachi F-2500 spectrophotometer instruments were employed for recording of UV–Vis absorption and fluorescence spectra, respectively. Electrochemical studies have been performed on a potentiostat (CH Instruments, Inc., USA; model 660D) at room temperature in anhydrous DMF containing 0.1 M TBAP (tetrabutylammonium perchlorate) as supporting electrolyte. A conventional three-electrode setup comprising of a glassy carbon working, Pt-wire auxiliary and Ag/AgCl reference electrode were used. During the experiment, the sample cell was deoxygenated by pursing nitrogen gas through the solution. Molar conductance measurement was recorded in properly calibrated on AQUASOL Digital Conductometer in DMF solution at 300 K. Electrospray ionization mass spectrometric (ESI–MS) measurement were recorded on a Waters Xevo G2-XS QTof mass spectrometer. The magnetic susceptibility at room temperature for the prepared complexes in solid state were recorded on Sherwood Scientific, Cambridge, England, employed $Hg[Co(NCS)_4]$ as magnetic susceptibility standard. The experimental susceptibility data have been corrected for the diamagnetic contribution of all the atoms and the sample holder using Pascal's tables. The time-resolved fluorescence lifetime measurement was carried out on a FSP920 fluorescence spectrometer (Edinburgh instrument) at 298 K. A Luzchem (model: LZC-1, Ontario, Canada) made photoreactor fitted with eight fluorescent white tubes (λ = 400–700 nm) was used for the experiments needing light exposure. A TECAN microplate reader (BioRad, Hercules, CA, USA) was used in MTT assays for recording absorbance of formazan. A BD Biosciences made FACS Verse flow cytometer fitted with a MoFLo XDP cell sorter and analyzer with three lasers (λ = 488, 365, and 640 nm) was used for flow cytometric experiments. Confocal microscopic images were acquired on a Leica laser scanning confocal microscope (TCS, SP5 DM6000) with an oil immersion lens with magnification of 63 × and the images were processed using LAS AF Lite software.

Synthesis

General procedure for Synthesis of $[Co(L)_2(Fc\text{-}cur)]ClO_4$ *(**1**, **2**) (L = phen, **1**; dppz, **2**).* Complexes **1** and **2** have been synthesized by a general procedure, where a methanolic solution (10 ml) of the respective phenanthroline bases [phen in **1** (0.20 g, 1 mmol) and dppz in **2** (0.29 g, 1 mmol)] were slowly added to a methanol solution of cobalt(II) acetate tetrahydrate (0.124 g, 0.5 mmol) and continuously stirred for 1 h at room temperature. The ligand Fc-curH (0.25 g, 0.5 mmol) deprotonated by one equivalent of dilute NaOH solution in methanol (15 ml) was added to the previous solution dropwise and stirred for another 1 h. The reaction mixture was filtered to remove any insoluble impurities and was treated with methanolic solution of $NaOCl_4.H_2O$. The brownish red precipitate was obtained after filtration was washed with cold methanol, water and finally dried in vacuo over anhydrous $CaCl_2$ (yield: 0.81 g, ~ 78% for **1**, 0.82 g, ~ 67% for **2**). (Scheme S1, Supporting information).

Anal. Calcd for $C_{51}H_{39}ClN_4O_6Fe_2Co$ (**1**): C, 60.65; H, 3.89; N, 5.55. Found: C, 60.39; H, 3.94; N, 5.67. Selected IR data (KBr phase, cm^{-1}): 1608 s (C=O), 1516 vs. (C=C), 1390 m, 1291 m, 1248 w, 1087 vs. (ClO_4), 1000 m, 966 w,

844 m, 716 w, 624 s (vs., very strong; s, strong; m, medium; w, weak). ESI–MS in MeCN: m/z=910.1028 $[M\text{-}ClO_4]^+$. UV–visible in DMSO in Tris–HCl buffer (1:9 v/v) (pH 7.2) [λ_{max}/nm (ε/M^{-1} cm^{-1})]: 269 (65,313), 390 (16,046), 535 (7,553). Λ_M = 76 S cm^2 mol^{-1} in DMF at 30 ºC. μ_{eff} = 4.72 µB at 298 K.

Anal. Calcd for $C_{63}H_{43}ClN_8O_6Fe_2Co$ (**2**): C, 62.32; H, 3.57; N, 9.23. Found: C, 62.13; H, 3.71; N, 9.29. Selected IR data (KBr phase, cm^{-1}): 1617 m (C=O), 1495 s (C=C), 1419 m, 1355 m, 1233 w, 1089 vs. (ClO_4), 822 w, 766 m, 733 m, 626 m. ESI–MS in MeCN: m/z = 1114.1431 $[M\text{-}ClO_4]^+$. UV–visible in DMSO in Tris–HCl buffer (1:9 v/v) (pH 7.2) [λ_{max}/nm (ε/M^{-1} cm^{-1})]: 276 (87,460), 363 (22,186), 380 (21,760), 530 (2766). Λ_M = 78 S cm^2 mol^{-1}at 30 ºC in DMF. μ_{eff} = 4.80 µB at 298 K.

*General procedure for Synthesis of [Co(L)$_2$(cur)]ClO$_4$ (**3**, **4**) (L = phen, **3**; dppz, **4**).* Complexes **3** and **4** were synthesized by a very similar procedure as described for complexes **1** and **2**. The ligand curH (0.5 mmol, 0.185 g) was used in lieu of Fc-curH. The brick-red precipitate obtained was washed with cold methanol, diethyl ether, water and finally dried in vacuo over anhydrous $CaCl_2$ (yield: 0.74 g, ~ 84% for **3**, 0.78 g, ~ 72% for **4**) (Scheme S1, Supporting information).

Anal. Calcd for $C_{45}H_{35}ClN_4O_{10}Co$ (**3**): C, 60.99; H, 3.98; N, 6.32. Found: C, 60.75; H, 4.11; N, 6.41. Selected IR data (KBr phase, cm^{-1}): 3400 br, 3062 w, 2928 w, 1625 m(C=O), 1588 s (C=C), 1509 vs., 1425 s, 1285 s, 1085 vs. (ClO_4), 976 w, 846 m, 725 m, 624 w (br, broad). ESI–MS in MeCN: m/z = 786.1833 $[M\text{-}ClO_4]^+$. UV–visible in DMSO in Tris–HCl buffer (1:9 v/v) (pH 7.2) [λ_{max}/nm (ε/M^{-1} cm^{-1})]: 268 (67,040), 430 (26,860). Λ_M = 75 S cm^2 mol^{-1} in DMF at 30 ºC. μ_{eff} = 4.74 µB at 298 K.

Anal. Calcd for $C_{57}H_{39}ClN_8O_{10}Co$ (**4**): C, 62.79; H, 3.61; N, 10.28. Found: C, 62.65; H, 3.77; N, 10.19. Selected IR data (KBr phase, cm^{-1}): 3425 br, 3081 w, 1617 m(C=O), 1575 s(C=C), 1497 s, 1419 m, 1355 m, 1234 w, 1085 vs. (ClO_4), 822 w, 766 m, 733 m, 624 m. ESI–MS in MeCN: m/z = 990.2206 $[M\text{-}ClO_4]^+$. UV–visible in DMSO in Tris–HCl buffer (1:9 v/v) (pH 7.2) [λ_{max}/nm (ε/M^{-1} cm^{-1})]: 274 (91,266), 367 (36,660), 380 (37,260), 436 (27,680). Λ_M = 80 S cm^2 mol^{-1} in DMF at 30 ºC. μ_{eff} = 4.82 µB at 298 K.

*Synthesis of [Co(phen)$_2$(acac)]ClO$_4$ (**5**).* Complex **5** was also synthesized by a very similar procedure as described for **1**–**4**. The ligand acacH (0.5 mmol, 52 µL) was used in lieu of Fc-curH or curH. The yellow precipitate obtained was washed with cold methanol, water and dried in vacuo over anhydrous $CaCl_2$. (yield: 0.87 g, ~ 87% for **5**) (Scheme S1).

Anal. Calcd for $C_{29}H_{23}ClN_4O_6Co$ (**5**): C, 56.37; H, 3.75; N, 9.07. Found: C, 56.11; H, 3.65; N, 9.21. Selected IR data (KBr phase, cm^{-1}): 1582 s (C=O), 1516 s (C=C), 1423 s, 1260 m, 1223 w, 1098 vs. (ClO_4), 925 w, 850 s, 780 m, 727 s, 622 s. ESI–MS in MeCN: m/z = 518.1071 $[M\text{-}ClO_4]^+$. UV–visible in DMSO in Tris–HCl buffer (1:9 v/v) (pH 7.2) [λ_{max}/nm (ε/M^{-1} cm^{-1})]: 268 (92,473). Λ_M = 85 S cm^2 mol^{-1} in DMF at 30 ºC. μ_{eff} = 4.50 µB at 298 K.

X-ray crystal structure determination

Dark red block shaped single crystals of [Co(phen)$_2$(acac)] ClO_4 (**5**) suitable for X-ray diffraction were obtained from slow evaporation of methanolic solution of the compound for 2 days. A crystal was mounted on the tip of a glass fibers with epoxy cement. Crystallographic data were collected on a Bruker SMART APEX II CCD diffractometer equipped with a Mo-$K_\alpha$fine focus sealed tube X-ray source (λ = 0.71073 Å) at 293 K. An empirical technique SADABS was employed to correct the intensities for absorption [41]. The direct methods Bruker SHELXTL program was used to solved the crystal structure and for the refinements. All the hydrogen atoms were refined isotropically, whereas for the non-hydrogen atoms were refined as anisotropically [42]. The perspective view of the molecule was obtained by ORTEP. Crystallographic information file (cif) is deposited in the CCDC (deposition no. 2050589) and may be accessed at the website www.ccdc.cam.ac.uk/data.

DNA binding method

The ability of the complexes **1**–**5** (15 µM) to bind to *ct*-DNA (235 µM; M.W. = 10–15 million daltons) was evaluated using UV–visible absorption titration experiment in DMSO-Tris–HCl buffer (pH 7.2). The intrinsic binding constant values were calculated using McGhee–von Hippel (MvH) method by recording the changes in absorption spectral bands at ~ 270 nm with increasing DNA concentration following literature procedures [43, 44].

HSA binding studies

The interaction of the complexes **1**–**5** with human serum albumin (HSA) in Tris–HCl buffer (pH 7.2) was assessed by tryptophan fluorescence quenching experiment [45]. The emission intensity of HSA (2 µM) at 340 nm was monitored upon excitation at 280 nm with increasing concentration of the complexes. The binding constants (K_{HSA}) were calculated using the equation $I_0/I = 1 + K[Q]$, where I_0 and I are the intensities of emission of HSA in absence and in presence of the quencher Q. Furthermore, we investigated to the HSA–metal complex interaction in terms of the static or dynamic nature of mechanism of fluorescence quenching by comparing the fluorescence lifetime measurement of HSA alone and in presence of two different concentrations (5 and 10 µM) of complex **2** in Tris–HCl buffer (pH 7.2) [46].

Determination of lipophilicity

A modified "shake-flask" methods was used to have an estimate of the lipophilicity of the complexes **1**–**5** in terms of their ability to partition (*P*) between n-octanol and water phases (expressed as log*P*) [47]. Briefly, 5 ml complex solution in octanol-saturated water is vortexed with 5 ml water-saturated octanol in a tube for ~ 20 min. The tube having the above solution was centrifuged for ~ 8–10 min at 3500 rpm, whereby the binary mixture separates out. The concentration for the complexes **1**–**5** in these two phases is calculated using UV–Vis spectroscopy. The partition coefficients are calculated using the equation $\log P = \log\{[\mathbf{1}\text{–}\mathbf{5}]_{oct}/[\mathbf{1}\text{–}\mathbf{5}]_{aq}\}$. Log*P* is expressed as average of three different complex concentrations.

Cellular experiments

The visible light induced cytotoxicity of the complexes **1**–**5** and other cellular experiments showing uptake of the complexes, species responsible for cell death, mechanism of cell death, cell cycle analysis etc. were performed using standard protocols. The cellular assays performed are briefly presented below:

(i) MTT Assay: The visible light induced cytotoxicity of the complexes **1**–**5** in HeLa (cervical carcinoma), A549 (human lung cancer cells) and HPL1D (immortalized peripheral lung epithelial cells) cells were studied by MTT assay [48]. The cells plated in 96 well plates were treated with different concentrations of the complexes **1**–**5** (100–3.13 μM) in triplicate. The experiments were performed in two sets, one for dark and one for light treatment, and incubated for 4 h. The media are discarded, and cells are suspended in phosphate buffer (50 mM, pH 7.4) having 150 mM NaCl (PBS). One plate is exposed to visible light (400–700 nm, 10 Jcm^{-2}) for 1 h in a photoreactor and the other plate is kept in dark covered with aluminium foil. PBS is replaced by DMEM and incubated for another 19 h in dark to keep the total time for the assay 24 h. After that, 25 μL of thiazolyl blue tetrazolium bromide (MTT) (4 mg mL^{-1}) was added to each well and incubated for another 4 h. The supernatants were aspirated and the purple formazan crystals settled at the bottom were dissolved in DMSO. The absorbance at each well was recorded at 570 nm in a microplate reader. The half maximal inhibitory concentration (IC_{50}) values were calculated by non-linear regression analysis using GraphPad Prism 8.

(ii) Confocal Microscopy: Confocal microscopic technique was employed to study the uptake and localization of the complexes of the curcumin containing complexes **3** and **4** [49]. ~ 4×10^4 A549 cells plated on cover slips were incubated with the complexes for **3** and **4** (10 μM) for 4 h. The media are discarded, washed with PBS and fixed using 4% paraformaldehyde for 10 min at room temperature. The cells were incubated with PI solution (50 μg/mL RNase A, 20 μg/mL PI in PBS) for 1 h at 42 ºC after washing with PBS. This was followed by another wash with PBS to remove excess PI. Cells were mounted and images were recorded using confocal laser scanning microscope.

(iii) Cellular uptake by ICP-MS: The overall and specific organelle uptake of cobalt in A549 cells were estimated using ICP-MS technique using standard protocols [50, 51]. Approximately 10^6 A549 cells cultured in 60 mm dishes were treated with complexes **1**, **2** and **5** (10 μM) for 4 h. The medium was aspired and washed with DPBS. 300 μL of 70% HNO_3 was added to each dish to lyse the cells, cells were scrapped from the dishes, lysates were transferred to 15 mL tubes and allowed to stand for 15 min. The lysates were treated with 100 μL H_2O_2 followed by incubation at 55 °C for ~ 3 h. The lysates were finally diluted to 10 mL with 2% HNO_3 and analyzed by ICP-MS. The overall cobalt content in A549 cells were expresses as ng of Co per billion cells. The experiments were carried out in triplicates and normalized to untreated controls.

To quantify cobalt content in the nucleus and cytosol, approximately 10^6 A549 cells seeded in culture dishes were treated with **1**, **2** and **5** (10 μM) in dark for 4 h in two sets, medium was aspirated and washed with DPBS. One set was used for estimated of cobalt, while the other set was used for counting live cells using trypan blue method after trypsinization. The cells were lysed using the detergent NP40 (0.5%) and the lysates were centrifuged at 12,000 g at 4 °C for 10 min. The supernatant cytosolic fraction was separated from the nuclear pallet. The nuclear pallet was then washed with DPBS to remove traces of the cytosolic faction. Both the fractions were re-suspended in 70% HNO_3 and H_2O_2 and incubated at 55 °C for ~ 3 h. The lysates were then diluted to 10 mL with 2% HNO_3 and cobalt was estimated by ICP-MS analysis.

To estimate the cobalt content in the mitochondrial fraction, approximately 10^6 A549 cells plated in 60 culture dishes were treated with **1**, **2** and **5** (10 μM) in dark for 4 h. The medium was discarded, and the cells were washed with DPBS. The cells were thoroughly scrapped from the dishes with a scraper, suspended in 15 mL tubes and centrifuged at 600 g at 4 °C for 10 min. The supernatant was discarded and the cells were re-suspended in mitochondrial isolation buffer IB [10 ml of 0.1 M tris(hydroxymethyl)aminomethane (Tris)/3-(N-morpholine) propanesulfonic acid and 1 ml of ethylene glycol-bis(b-aminoethyl ether)-*N*,*N*,*N*',*N*'-tetraacetic acid/Tris to 20 ml of 1 M sucrose and volume made up to 100 ml (pH 7.4) and 1 ml EGTA/Tris to 20 ml of 1 M sucrose and volume made up to 100 ml (pH = 7.4)]. The homogenization of the cells was carried out at 4 °C using a Teflon pestle at 1600 rpm. The cell suspensions were then stroked gently using a glass potter cooled in ice-bath to

maintain the mitochondrial integrity. The homogenate was centrifuged at 600 g at 4 °C for 10 min, the supernatant was collected and centrifuged again at 7000*g* at 4 °C for 10 min. The pellets obtained were washed with 200 µl of ice-cold isolation buffer IB after discarding the supernatant. The homogenates were further centrifuged at 7000*g* at 4 °C for 10 min and the mitochondrial pellets were collected. The pellets were re-suspended in 70% HNO_3 and H_2O_2 and incubated at 55 °C for ~ 3 h, diluted to 10 mL with 2% HNO_3 and were used for estimation of cobalt by ICP-MS technique. Another such set was used for measuring the concentration by Biuret methods and examining the separation of mitochondria by gel electrophoresis.

(iv) DCFDA Assay: DCFDA assay was employed to evaluate the ability of the active complex **2** (5 µM) to generate ROS on exposure to visible light [52]. A549 cells treated with complexes **2** for 4 h followed by a treatment with DCFDA (1 µM) for 5 min were exposed to visible light (400–700 nm, 10 Jcm^{-2}) in PBS in a photo-reactor. The corresponding dark control experiments were carried out. The cells were harvested by trypsinization and the distribution of fluorescent DCF in the cells was evaluated by flow cytometry and data were processed using Cyflogic V software.

(v) Annexin V-FITC-PI Assay: The apoptotic or necrotic nature of cell death induced by the complexes **2** and **5** in A549 cells was assessed by Annexin V-FITC-PI assay [53]. The cells were treated with **2** and **5** (5 µM) for 4 h followed by exposure to visible light (400–700 nm, 10 Jcm^{-2}) for 1 h in PBS. Suitable dark controls experiments are performed. The cells are further incubated for 19 h in DMEM/10% fetal bovine serum (FBS) buffer in dark. The cells were harvested by trypsinization and suspended in Annexin V binding buffer (140 µL; 100 mM HEPES/NaOH, pH 7.4 having 140 mM NaCl and 2.5 mM $CaCl_2$). The suspensions were incubated with FITC conjugated Annexin V (0.5 mL) and PI (5 µM, 1 mL) and analyzed flow cytometrically.

Results and discussion

Synthesis and general aspects

Two Co(II) complexes having ferrocene-based curcuminoid ligand (Fc-curH), namely, $[Co(L)_2(Fc\text{-}cur)]ClO_4$ (**1**, **2**), where L is 1,10-phenanthroline (phen in **1**) and dipyrido[3,2-a:2',3'-c]phenazine (dppz in **2**) were synthesized in good yields using a simple synthetic procedure at room temperature in air. To understand the efficacy of the Fc-cur ligand in coordinated form to Co(II) as photochemotehrapeutic agents, two Co(II) curcumin (curH) complexes viz. $[Co(L)_2(cur)]ClO_4$ (**3**,**4**), where L is phen (in **3**) and dppz (in **4**) were synthesized in an efficacious way. The complex $[Co(phen)_2(acac)]ClO_4$ (**5**), where acacH is acetylacetone is synthesized, structurally characterized and used a control compound in understanding the light-induced chemotherapeutic potential of **1**–**4**. All the compounds were fully characterized using various spectral and analytical techniques. Selected physicochemical data are given in Table 1. Fc-curH was characterized by ^1H NMR and mass spectral analysis (Figs. S1 and S2, Supporting information). Satisfactory elemental analysis data are observed for complexes synthesized. The ESI mass spectra of the complexes in acetonitrile displayed a base peak assignable to the $[M\text{-}(ClO_4)]^+$ species which corroborate the solution phase stability of the complexes (Fig. S3–S7, Supporting information). Complexes **1**–**5** are 1:1 electrolyte displaying molar conductance value at ~ 78 Scm^2mol^{-1} in DMF at 298 K that do not change significantly over time. This indirectly shows

Table 1 Selected Physicochemical Data for the Complexes $[Co(L)_2(Fc\text{-}cur)]ClO_4$ (**1**, **2**), $[Co(L)_2(cur)]ClO_4$ (**3**, **4**) and $[Co(L)_2(acac)]ClO_4$ (**5**) (L = phen, **1, 3, 5**; dppz, **2, 4**)

Complex	IR[a]/cm^{-1} ν(C=O),ν(C=C), $\nu(ClO_4^-)$	λ_{max}/nm (ε / M^{-1} cm^{-1})[b]	E_f/V(ΔE_p/mV)[c] Co(II)–Co(I), Fc–Fc^+	μ_{eff}[d]/ μ_B	Log$P_{o/w}$
1	1608, 1516, 1087	269 (65,313), 390 (16,046), 535 (7,553)	− 0.98 (76), 0.40 (69)	4.72	0.84
2	1617, 1495, 1089	276 (87,460), 363 (22,186), 380 (21,760), 530 (2,766)	− 0.95 (162), 0.42 (76)	4.80	1.10
3	1625, 1588, 1085	268 (67,040), 430 (26,860)	− 0.98 (93), –	4.74	0.56
4	1617, 1575, 1085	274 (91,266), 367 (36,660), 380 (37,260), 436 (27,680)	− 0.99 (91), –	4.82	0.89
5	1582, 1516, 1098	268 (92,473)	− 1.02 (83), –	4.50	− 0.08

[a]In KBr phase. [b]In DMSO-Tris–HCl buffer (pH 7.2) (1:9 v/v). [c]Co(II)–Co(I) couple in DMF–0.1 M TBAP, $E_f = 0.5(E_{pa} + E_{pc})$, $\Delta E_p = (E_{pa} — E_{pc})$, where E_{pa} and E_{pc} are the anodic and cathodic peak potentials, respectively. The potentials are vs. Ag/AgCl electrode. Scan rate = 50 mV s^{-1}. [d]Magnetic moment at 298 K

solution phase stability of the complexes with no ligand scrambling in solution resulting in the formation other species. The magnetic moment values of ~ 4.7 μB suggest that they are three electron paramagnetic high spin $3d^7$ Co(II) complexes (Table 1). The solid-state infrared spectra for the complexes give characteristic stretching frequencies around at ~ 1610 cm^{-1} and ~ 1540 cm^{-1} for C=O and C=C bands, respectively. Moreover, a strong IR band at ~ 1080 cm^{-1} was observed for all the metal complexes due to the presence of ClO_4^- counter ion (Figs. S8–S12, Supporting information). The UV–visible spectra for the complexes were recorded in DMSO-Tris–HCl buffer (1:9 v/v, pH 7.2) displayed a higher energy intense band ~ 265–275 nm due to $\pi \rightarrow \pi^*$ transition of the phenanthroline bases (Fig. S13, Supporting information). **2** and **4** containing dppz ligand showed two extra peaks at ~ 360–380 nm due to $n \rightarrow \pi^*$ transition dppz ligand. A moderately intense visible absorption band was observed for the curcumin complexes **3** and **4** at ~ 430 nm due to $\pi \rightarrow \pi^*$ of curcumin. Complexes **1** and **2** having Fc-cur ligand displayed two broad bands in the visible region, one at ~ 400 nm due to $\pi \rightarrow \pi^*$ transition of the conjugated -C = C- bonds and the other at ~ 520 nm due to $^1A_{1g} \rightarrow {}^1E_{1g}$ transition of the ferrocene moiety (Fig. 1) [54]. In all the complexes, except **5**, d–d bands due to Co(II) center were masked due to intense ligand-centered bands in visible region. Co(II)–curcumin complexes **3** and **4** emit in green at ~ 520 nm upon excitation at ~ 440 nm in DMSO-Tris–HCl buffer (pH 7.2) (1:9 v/v), whereas the Fc-cur complexes **1** and **2** were non-fluorescent in nature (Fig. S14, Supporting information). The curcumin-based emission intensity of the complexes at ~ 520 nm is significantly quenched compared to free curcumin due to coordination to paramagnetic

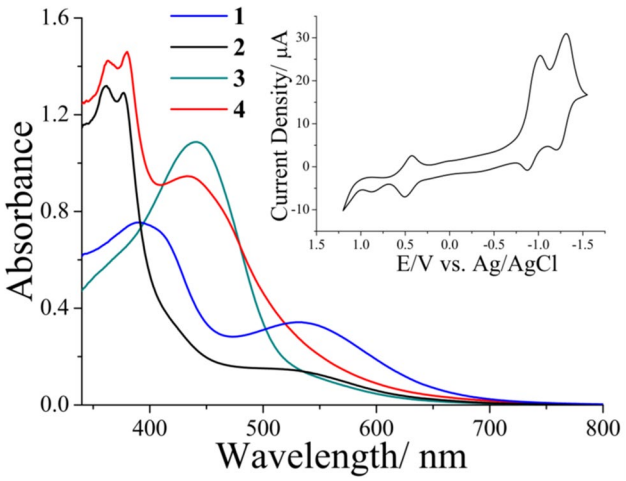

Fig. 1 UV-visible spectra of $[Co(L)_2(Fc\text{-}cur)]ClO_4$ (**1**, **2**) and $[Co(L)_2(cur)]ClO_4$ (**3**, **4**) (L = phen in **1** and **3**; dppz in **2** and **4**) (25 μM) in DMSO-Tris-HCl buffer (pH 7.2) (1:9 v/v). The inset shows selected cyclic voltammetric responses of **2** in DMF

$3d^7$-Co(II) center. However, unlike the curcumin complexes, complexes **1** and **2** having Fc-cur ligand did not show any emission upon electronic excitation. The complexes **1** and **2** having Fc-cur ligand showed quasi-reversible cyclic voltammetry responses for the Co(II)/Co(I) and Fc–Fc^+ couples at ~ -1.0 and 0.45 V, respectively, against Ag/AgCl reference electrode in DMF-0.1 M TBAP. An irreversible voltammetry response corresponding to Co(III)/Co(II) couple was observed at ~ 0.87 V for **2**, whereas the same was not prominent for **1** probably due to Fc–Fc^+ couple with higher current density. The curcumin complexes **3** and **4** displayed quasi-reversible responses for the Co(II)/Co(I) couple at ~ − 1.0 V and irreversible responses for the Co(III)/Co(II) couple at ~ 0.8 V. A curcumin-centered oxidation peak is also observed at ~ 0.22 V in both **3** and **4**. The dppz ligand also shows a quasi-reversible redox signals at ~ − 1.3 V in complexes **2** and **4** (Fig. 1, Fig. S15, Supporting information).

Solubility and stability

The complexes **1**–**5** are moderately soluble in a wide variety of solvents, such as methanol, ethanol, acetonitrile, tetrahydrofuran, nitromethane etc., **1**–**5** are highly soluble in DMF and DMSO and their aqueous solution, but insoluble in toluene, hexane and other hydrocarbons. Time dependent solution phase stability of the complexes studied by recording their electronic absorption spectra in DMSO-Tris–HCl buffer (1:9 v/v) (pH 7.2) over a period of 24 h. The complexes **1** and **2** having Fc-cur ligand displayed remarkable stability in the time period of study with no significant change in their UV–visible spectra. The Co(II) curcumin complexes **3** and **4** were also significantly stable under similar experimental condition with minor decrease in the absorption spectra (Fig. S16, Supporting information). However, free curcumin is known to undergo almost complete degradation in 24 h time period at physiological pH [55]. This indicates that the Co(II) complexes of ferrocene-based curcuminoid is highly stable at physiological pH and expected to overcome the instability and bioavailability issues associated with the formulation of curcumin for potential biomedical applications. We also checked photo-stability of the complexes in visible light. Ferrocene compounds are reported to undergo oxidation to ferrocenium species when exposed to visible light [56]. However, the compounds **1** and **2** did not show significant oxidation when exposed to visible light for a period of 30 min (Figure S17, Supporting information).

X-ray crystal structure

The solid-state structure of $[Co(phen)_2(acac)]ClO_4$ (**5**) was determined by single crystal X-ray crystallographic technique using suitable crystals grown from methanol. The crystal belongs to *C*2/c space group of monoclinic crystal

system with cell parameters $a = 32.386(3)$, $b = 10.2910(8)$, $c = 17.2217(12)$ Å and $\beta = 107.179(5)^{\circ}$. The refinement converged to $R = 0.0593$, $wR = 0.1475$ and goodness of fit 0.980. The asymmetric unit contains one complete molecule of complex **5** and there are 8 molecules in the unit cell. (Fig. S18, Supporting information). An ORTEP of the molecule is shown in Fig. 2. Selected crystallographic parameters are shown in Table S1 (Supporting information). The structure adopts an octahedral geometry around the Co(II) center with CoN_4O_2 coordination mode chelated by two phenanthroline and one acetylacetonate ligands. The average Co–N and Co–O distances are 2.149 and 2.044 Å, respectively. The selected bond distances and bond angles are given in Table S2 (Supporting information).

DNA Binding studies

UV–visible titration experiments are performed to evaluate the affinity of the complexes to *ct*-DNA. The changes in the electronic spectral features of the complexes **1**–**5** (15 µM) upon addition of *ct*-DNA (235 µM) are shown in Figure S19 (Supporting information). It is evident that the complexes display significant hypochromism with minor bathochromic shift of the $\pi \rightarrow \pi^*$ transition bands of the phenanthroline bases. The complexes **2** and **4** having flat planar extended aromatic dppz ligand showed ~ 25–38% of hypochromicity of the band at 275 nm, whereas the phenanthroline complexes **1**, **3** and **5** gave ~ 11–13% hypochromicity when titrated with DNA solution. The data fitted to Von-Hippel equation gives the binding constant (K_b) values in the order: **2** > **4** > **3** > **5** > **1** (Table S3, Supporting information). The complexes **2** and **4** displayed K_b value of the order

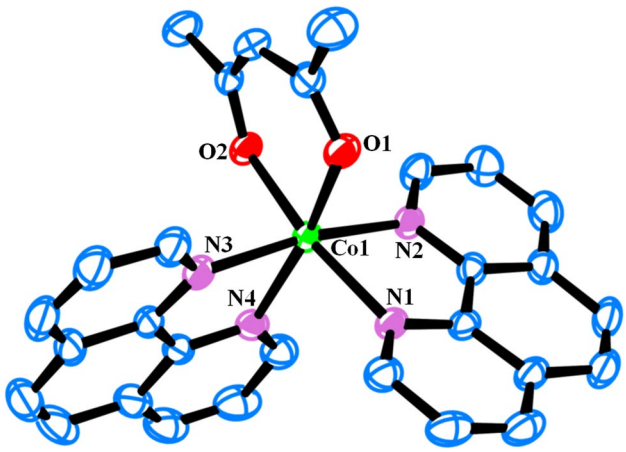

Fig. 2 ORTEP of complex **5** showing 30% probability thermal ellipsoids with the atom-numbering scheme for the metal and heteroatoms. The hydrogen atoms and counter ion are omitted for clarity [Color code: carbon, blue; nitrogen, orchid; oxygen, red; cobalt, green]

10^5–10^6 M^{-1}, whereas the complexes **1**, **3** and **5** exhibited 10^4–10^5 M^{-1} order of binding constants. We believe that the Co(II) dppz complexes interact with *ct*-DNA primarily via intercalation of the dppz ligand [57]. Lower K_b values indicate that the 1,10-phenanroline complexes are most likely to be groove binders probably with partial intercalation.

Binding behavior to protein

Human serum albumin (HSA) is the most abundant plasma protein that binds and transports various endogenous and exogenous small molecules in the plasma. It is widely recognized that the serum albumin can reversibly bind drug molecules to affect their distribution in tissues resulting in its increased importance in targeted delivery [58]. The HSA binding propensities of the complexes **1**–**5** were studied with the aid of fluorescence quenching experiments by monitoring emission intensity of HSA due to the single tryptophan residue (Trp-214) in Tris–HCl buffer (pH 7.2). The emission intensity of HSA at ~ 340 nm upon excitation on 280 nm was observed to be gradually decreasing along with minor blue shift with increasing the complex concentration. The data were fitted to the equation $I_0/I = 1 + K[Q]$, where I_0 and I are the emission intensity of HSA in the absence and in the presence of quencher of concentration [Q], respectively (Fig. S20, Supporting information). The binding constant values (K_{HSA}) were determined from the slope of the plots and found to follow the order: **2** > **4** > **1** ~ **3** > **5** (Table S3, Supporting information). The complexes show moderate binding affinity for HSA having the binding constants of the order of ~ 10^4–10^5 M^{-1}. Complexes **2** and **4** were found to display higher binding constants compared to their phenanthroline analogues **1** and **3**. This could be due to higher affinity of the complexes **2** and **4** to some hydrophobic pockets in the protein. We were interested in evaluation of the fluorescence quenching mechanism of HSA by the complexes, i.e., whether they form ground state complexes with has, i.e., static or the quenching mechanism involves excited electronic states, i.e., dynamic in nature. UV–visible spectra for HSA in presence of complexes **1** and **2** in DMSO-Tris–HCl buffer (1:9 v/v, pH 7.2) show changes the absorption spectra of HSA with a minor blue shift (~ 3 nm) for **1** and red shift (~ 6 nm) for **2** (Fig. S21, Supporting information). This is believed to be the result of ground state complexation of protein with complexes that indicates static mechanism of fluorescence quenching. Further to confirm the static mechanism of fluorescence quenching of HSA by the complexes, we recorded fluorescence life-time HSA alone and upon addition of complex **2** (10 µM). No significant changes in fluorescence lifetime of HSA is observed in presence of complex **2** which indicates that the interaction between the serum protein and complex **2** happens in the ground state (Fig. S22, Supporting information) [59].

Lipophilicity measurement

Measurement of lipophilicity of a drug candidate is extremely important as it often correlated to cell permeability, absorption, distribution, metabolism and excretion of a drug [60]. We have measured the lipophilicity of the complexes **1**–**5** in terms of their partition coefficient (*P*) between water and n-octanol and expressed as log*P*. The lipophilicity order has been found to be **2** > **4** > **1** > **3** > **5** (Table 1). The trend suggest that the Co(II) ferrocenyl curcuminoid complexes are significantly more lipophilic compared to their curcumin analogues. Ferrocene compounds are getting increased attention as pharmacophores due to its various exciting properties among which lipophilicity is one of the major one as exemplified by the success of ferrocene as anticancer and ferroquine antiplasmoidal agents. Therefore, use of ferrocene as bioisostere for the two aryl groups of curcumin is expected to enhance the uptake of these Co(II) complexes in cancer cells resulting better photochemotherapeutic activity.

Photocytotoxicity study

Evaluation of photochemotherapeutic potential of the complexes **1**–**5** against cervical carcinoma (HeLa) and human lung cancer (A549) cells and human peripheral lung epithelial normal cells (HPL1D) was carried out using MTT assay (Fig. 3, Fig, S23–S26, Supporting information). The assay estimates the percentage of cell survival in presence of various concentrations of the complexes compared to control experiments and the results are expressed as half maximal inhibitory concentration (IC_{50}) values. The complexes **1** and **2** having ferrocene-based curcuminoid ligand (Fc-cur) display remarkable light-induced cytotoxicity in visible light in HeLa cells while displaying very low toxicity up to a much higher concentration in dark. The IC_{50} values for the complexes **1** and **2** are, respectively, 4.7 and 3.3 μM in light, whereas the IC_{50} values in dark are > 100 μM. Photoxicity indices (PI), which are defined as the ration of IC_{50} values in dark vs. light, are found to be > 21 and 30 for **1** and **2,** respectively. The complexes **1** and **2** are also found to be highly phototoxic to A549 cells displaying IC_{50} values of 3.5 and 2.1 μM, respectively, in visible light. The corresponding PI values of are ~ 26 and 41. This is highly desirable in designing photochemotherapeutic agents, whereby non-toxic compounds become lethal to cancer cells on shining light on them. As the ferrocene moieties in **1** and **2** do not undergo oxidation in visible light, we believe that photocytotoxicity is due to the generation of reactive oxygen species involving the Co(II) entre. The Co(II)–curcumin complexes **3** and **4** are also found to be significantly phototoxic to HeLa and A549 cells when exposed to visible light while being non-toxic to much higher doses in dark. The PI values for **3** and **4** are found to be > 10 and 21 in HeLa cells, whereas they are ~ 12 and 20 in A549 cells, respectively. The IC_{50} values of the complexes, curcumin and photofrin are shown in Table 2 [50, 61–63]. The higher light-induced toxicity for the Co(II) Fc-cur complexes could be due to their higher uptake in cancer cells owing to their higher lipophilicity. The lower dark toxicity of the Fc-cur complexes **1** and **2** compared to their curcumin analogues **3** and **4** could be due to their higher stability in cellular environment. Co(III)–curcumin

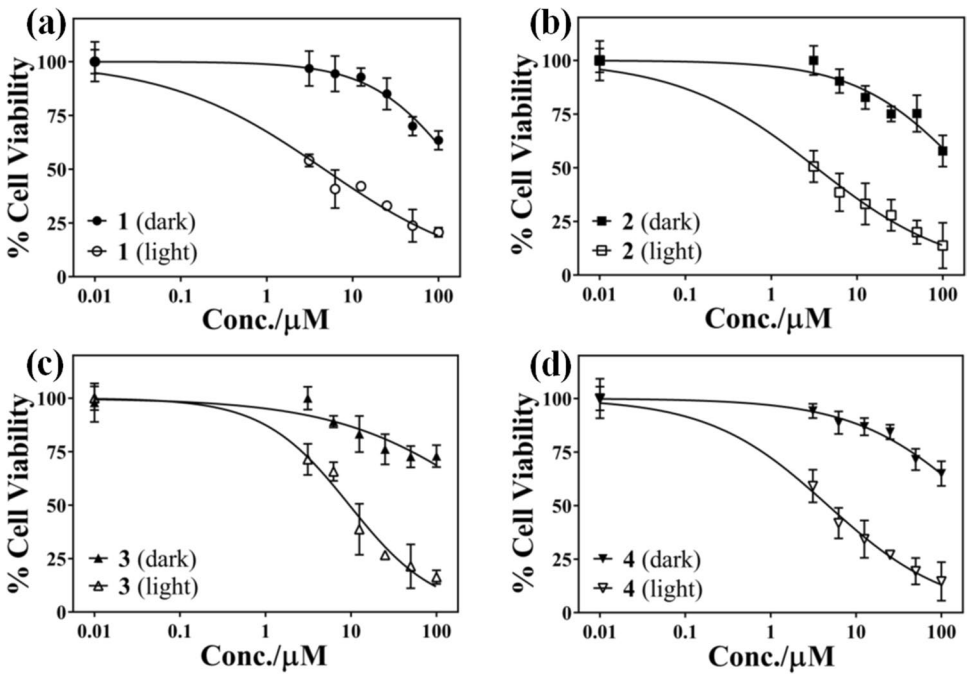

Fig. 3 Cell viability plots showing the cytotoxic effect of the complexes **1**–**4** in HeLa cells in dark (solid symbols) and in the presence of visible light (hollow symbols, 400–700 nm, 10 J cm^{-2}, 1 h)

Table 2 IC_{50} values of Photofrin®, curcumin, $[Co(L)_2(Fc\text{-}cur)]ClO_4$ (**1**, **2**), $[Co(L)_2(cur)]ClO_4$ (**3**, **4**) and $[Co(L)_2(acac)]ClO_4$ (**5**) (L = phen in **1**, **3** and **5**; dppz in **2** and **4**) in HeLa, A549 and HPL1D cells

Compound	IC_{50} (μM)								
	HeLa			A549			HPL1D		
	Dark[a]	Light[b]	PI[c]	Dark[a]	Light[b]	PI[c]	Dark[a]	Light[b]	PI[c]
1	> 100	4.7(± 0.7)	> 21.3	90(± 3.2)	3.5(± 0.5)	25.7	> 100	> 100	–
2	> 100	3.3(± 0.5)	> 30.3	86.7(± 3.0)	2.1(± 0.4)	41.3	> 100	83.5 (± 3.9)	> 1.2
3	> 100	9.6(± 0.8)	> 10.4	84.1(± 2.8)	6.7(± 0.6)	12.5	> 100	> 100	–
4	> 100	4.7(± 0.6)	> 21.7	72.2(± 2.2)	3.6(± 0.5)	20	> 100	76.6 (± 3.3)	> 1.3
5	> 100	> 100	_	> 100	83.6(± 3.1)	> 1.2	> 100	> 100	–
Curcumin	85.4(± 0.6)[d]	8.2(± 0.2)[d]	10.4	61.4(± 0.4)[e]	19 ± (0.9)[e]	3.2	> 100[e]	98.8(± 0.7)[e]	–
Photofrin®	> 41[f]	4.3(± 0.2)[f]	> 9.5	> 50[g]	0.5(± 0.04)[g]	> 100	–	–	–

[a]The IC_{50} values correspond to 4 h treatment followed by 20 h incubation in dark

[b]The IC_{50} values correspond to 4 h pre-incubation in dark followed by photo-exposure to visible light (400–700 nm, 10 J cm^{-2}, 1 h) and post incubation of 19 h in dark

[c]PI (Phototoxic Index) is the ratio between the IC_{50} values in the dark and visible light exposure

[d]IC_{50} values are taken from Ref [61]

[e]IC_{50} values are taken from Ref [50]

[f]IC_{50} values are taken from Ref [62]

[g]IC_{50} values are taken from Ref. [63] and correspond to irradiation for 30 min using a 50 W high-pressure Hg lamp followed by post incubation of 48 h in dark

complexes reported by Hussain et al. were also highly phototoxic, but significantly toxic in dark under similar conditions displaying low PI values [64]. The light vs. dark toxicity profiles of the Co(II) curcumin complexes **3** and **4** reported herein are superior to those of the Co(III) curcumin complexes reported earlier [64]. The higher dark toxicities of the Co(III) curcumin complexes could be due to the reduction of Co(III) to Co(II) with concomitant release curcumin under the reducing cellular environment at low oxygen concentration in cancer cells [64]. However, the cobalt complexes reported here are already in + 2 oxidation state thereby eliminating the possibility of electron transfer processes in dark which probably lowers their dark toxicity. Oxidation state of the cobalt center is found have significant effect on the dark toxicity of these compounds in HeLa and A549 cells. The control complex **5** having no ligand that can strongly absorb in visible region is not toxic at all in dark as well as visible light. This could also be the result of poor lipohilicity of the complex resulting in its inability to pass through the cell membrane of the cancer cells. The complexes **1**–**5** were found to be largely nontoxic to transformed human peripheral lung epithelial cells (HPL1D) in dark as well as visible light (Table 2, Figs. S25, S26 Supporting information).

Cellular uptake and localization

Cellular uptake and localization of anticancer drugs provide vital information for understanding of their potential cellular targets, mechanism of action and rational design of new molecules [65]. We took advantage of the curcumin-based residual fluorescence of Co(II) curcumin complexes **3** and **4** to study their uptake in A549 cells by confocal laser scanning microscopy (Fig. 4). The green fluorescence images due to the complexes **3** and **4** were recorded from A549 cells after co-staining the nuclei with propidium iodine. Merge images are presented in last panel which shows zone of overlay of green and red as pale orange color. Overlay of the images makes it evident that the two curcumin complexes primarily localize in the nucleus of A549 cells in 4 h along with minor cytosolic localization. This makes nucleic acids and other nuclear materials potential nuclear targets of these molecules for inducing cell death via photodynamic action.

The uptake of the non-fluorescent Co(II)–Fc-cur complexes **1** and **2** were studied by ICP-MS technique and expressed as ng of cobalt per billion A549 cells [50]. These results are compared with the control complex **5**. Cells treated with 10 μM complex concentration for 4 h in dark displayed an uptake of 127.5 and 118.3 ng of cobalt/10^6 cells for **1** and **2,** respectively (Table S4, Supporting information). The control complex **5** with poor lipophilicity did not show significant uptake (13 ng of cobalt/10^6 cells) in A549 cells under similar assay conditions. It is observed that the ferrocene–appended cobalt complexes were significantly internalized over a short span of time in A549 cells. The sub-cellular distribution of the cobalt complexes was further estimated in the nucleus and mitochondria of A549 cells. The nuclear fraction isolated from A549 cells treated with **1** and **2** (10 μM) showed an estimate of 81.7 and 75.2 ng of

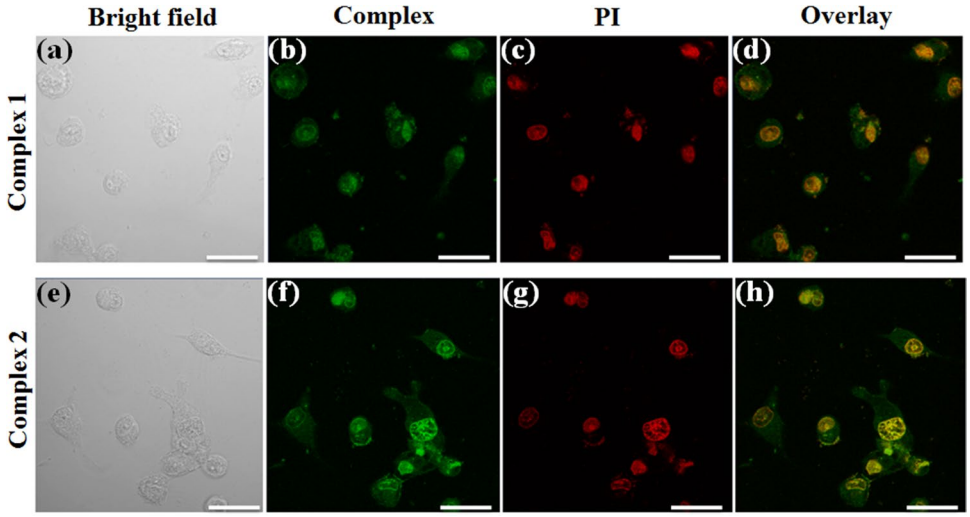

Fig. 4 Confocal microscopic images of A549 cells treated with the curcumin complexes **3** (**a**–**d**) and **4** (**e**–**h**) (5 μM) for 4 h and propidium iodide (PI). Panels (**a**) and (**e**) correspond to bright field images. Panels (**b**) and (**f**) correspond to the green emissions of **3** and **4** upon excitation with 405 nm laser. Panels (**c**) and (**g**) correspond to the red emission of PI. Panels (**d**) and (**h**) are the merged images of the first two panels. The scale bar in panel (**a**) corresponds to 20 μm

cobalt per billion cells, respectively, whereas the mitochondrial fraction displayed the respective uptake of 40.5 and 37.3 ng of cobalt per billion cells (Table S5, Supporting information). Form the above results it can be inferred that the Fc-cur cobalt complexes localize in the nucleus of A549 cells in significantly higher proportion.

Detection of ROS generation by flow cytometry

DCFDA (2',7'-dichlorofluorescin diacetate) was used to detect intracellular ROS level on light exposure in the complex treated cells compared to various control experiments [66]. Metal complexes are known to control generation ROS by thereby regulating the fate of the cells. DCFDA is used as a fluorescent probe to detect cellular ROS. Non-fluorescent DCFDA is deacylated by cellular esterases to H_2DCF which is subsequently oxidized to fluorescent DCF (2',7'-dichlorofluorescein) by intracellular ROS. Therefore, more the ROS generated more will be the fluorescence intensity due to formation of DCF. The process can be detected by flow cytometry using FL-1 green channel. We investigated visible-light induced ROS generation ability of the complex **2** (5 μM) in A549 cells and compared to control experiments in dark under similar assay conditions. There significant increase in ROS generation by both the complexes on light irradiation compared to cells treated with the complexes in dark (Fig. 5). The results infer that ROS is primarily responsible for cell death induced by the complexes under light exposure.

Mechanism of cell death

Annexin V-FITC conjugate can be used a fluorescent probe along with nucleic acid co-stain PI to identify the mechanism of cell death, i.e., apoptosis or necrosis [67]. Apoptosis is programmed cell death which is naturally controlled,

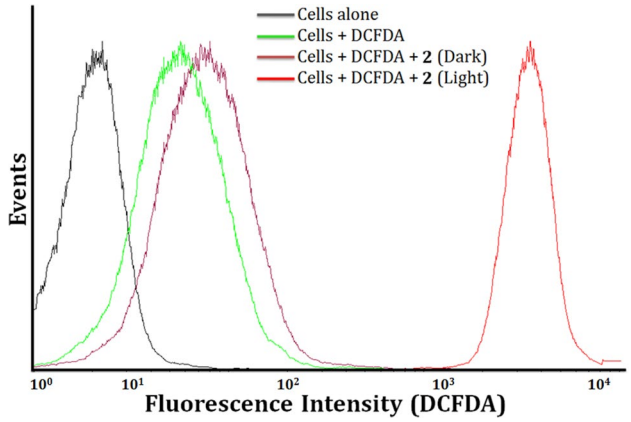

Fig. 5 Flow cytometry to detect the generation of ROS in A549 cells using DCFDA assay for complex **2** (5 μM) under different experimental conditions shown in color codes: cells only (black); cells + DCFDA (green); cells + DCFDA + complex **2** (in dark) (brown); cells + DCFDA + complex **2** (in light) (red). A greater shift in fluorescence intensity implies higher amount of DCF and greater ROS generation

regulated and highly desirable in designing cytotoxic agents as anticancer agents. Early apoptosis process starts with translocation of phosphatidylserine present on the interior of cell membrane to the exterior. Annexin V protein can selectively bind to this membrane lipid and the event can be detected using FITC tagged annexin V. In the late stage of apoptosis membrane integrity is lost and membrane becomes permeable to propidium iodide which fluoresce in red on binding to DNA. We used complex **2** to check cell death mechanism induced on light exposure in A549 cells. Figure 6 shows the dot plot obtained from flow cytometry using FL-1 and FL-2 channels for Annexin V-FITC and PI, respectively. The lower left quadrant depicts the percentage population of healthy cells, whereas the lower right, upper right and upper left quadrants give the population of cells

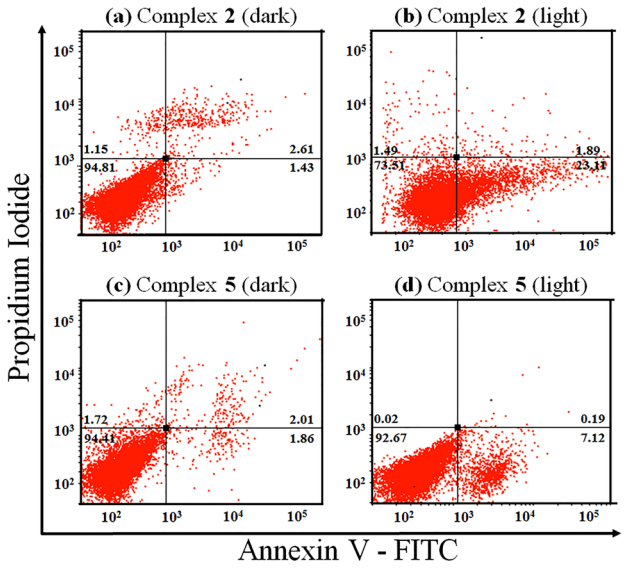

Fig. 6 Annexin V-FITC-PI staining of A549 cells showing the apoptosis induced by complexes **2** and **5** (5 μM) in dark and visible light (400–700 nm, 10 Jcm^{-2}) analyzed by flow cytometry

in early apoptosis, late apoptosis and necrosis, respectively. A549 cells treated with complex **2** for 4 h in dark followed by incubation in dark for 20 h did not induce significant cell death compared to untreated controls. However, A549 cells treated with complex **2** for 4 h followed by 1 h exposure to visible light (400–700 nm, 10 Jcm^{-2}) resulted in significant cell death after 24 h (Fig. 6). ~ 23% of the total population of cells were found to be in early apoptosis stage, whereas ~ 2% and 1.5% were in late apoptosis and necrosis stages, respectively. Control experiments using complex **5** did not show any significant induction of apoptosis in A549 cells in dark as well as visible light. The observation makes it clear that complex **2** kills A549 cells essentially via apoptosis mechanism only when exposed to visible light.

Conclusion

Highly stable Co(II) complexes having a lipophilic ferrocene-based curcuminoid have been designed as photochemotherapeutic agents and their activities compared to the corresponding Co(II) curcumin complexes. The complexes display significant binding affinity to calf-thymus DNA. They also have moderate binding propensity for the most abundant plasma protein human serum albumin which could potentially act as carrier for the molecules. In vitro studies show that the Fc-cur complexes are excellent photochemotherapeutic agents in human cervical and lung cancer cells with amazing phototoxic indices. They are found to be superior to their curcumin analogues in terms of light-induced anticancer activities. The complexes can generate ROS on electronic excitation of the bands in visible region. The primary mechanism of cell death is found to be ROS mediated apoptosis under visible light illumination. The present investigation opens a new class of molecules having organometallic pendants for the design and development of highly effective photocytotoxic agents for cancer therapy.

Supplementary Information The online version contains supplementary material available at https://doi.org/10.1007/s00775-021-01899-z.

Acknowledgements We are greatful to Department of Science and Technology (DST) INSPIRE Program, Government of India for financial support (IFA14-CH-164). The authors thank DST and Department of SAIF, Gauhati University for a CCD difractometer facility. We are thankful to Dr. Ranjit Thakuria for his kind help in X-ray crystallographic procedures. The authors sincerely thank Prof. A. R. Chakravarty, Indian Institute of Science, Bangalore for allowing us to use his cell culture facility.

Declarations

Conflict of interest The authors declare no conflict of interest.

References

1. Johnstone TC, Suntharalingam K, Lippard SJ (2016) Chem Rev 116:3436–3486
2. Kelland L (2007) Nat Rev Cancer 7:573–584
3. Gibson D (2009) Dalton Trans 10681–10689
4. Oun R, Moussa YE, Wheate NJ (2018) Dalton Trans 47:6645–6653
5. Galluzzi L, Senovilla L, Vitale I, Michels J, Martins I, Kepp O, Castedo M, Kroemer G (2012) Oncogene 31:1869–1883
6. Kwiatkowski S, Knap B, Przystupski D, Saczko J, Kędzierska E, Knap-Czop K, Kotlińska J, Michel O, Kotowski K, Kulbacka J (2018) Biomed Pharmacother 106:1098–1107
7. Allison RR, Moghissi K (2013) Clin Endosc 46:24–29
8. Zhang J, Jiang C, Longo JPF, Azevedo RB, Zhang H, Muehlmann LA (2018) Acta Pharm Sin B 8:137–146
9. Kou J, Dou D, Yang L (2017) Oncotarget 8:81591–81603
10. O'Connor AE, Gallagher WM, Byrne AT (2009) Photochem Photobiol 85:1053–1074
11. Moriwaki SI, Misawa J, Yoshinari Y, Yamada I, Takigawa M, Tokura Y (2001) Photodermatol Photoimmunol Photomed 17:241–243
12. Wang X, Wang X, Jin S, Muhammad N, Guo Z (2019) Chem Rev 119:1138–1192
13. Monro S, Colón KL, Yin H, Roque J, Konda P, Gujar S, Thummel RP, Lilge L, Cameron CG, McFarland SA (2019) Chem Rev 119:797–828
14. Reeßing F, Szymanski W (2017) Curr Med Chem 24:4905–4950
15. Liu J, Zhang C, Rees TW, Ke L, Ji L, Chao H (2018) Coord Chem Rev 363:17–28
16. Heinemann F, Karges J, Gasser G (2017) Acc Chem Res 50:2727–2736
17. Pandey V, Raza MK Joshi P, Gupta I (2020) J Org Chem 85:6309-6322
18. Imberti C, Zhang P, Huang H, Sadler PJ (2020) Angew Chem Int Ed 59:61–73

19. Fernandez-Moreira V, Gimeno MC (2018) Chem Eur J 24:3345–3353
20. Ramu V, Gautam S, Kondaiah P, Chakravarty AR (2019) Inorg Chem 58:9067–9075
21. Zhang P, Sadler PJ (2017) J Organomet Chem 839:5–14
22. Gasser G, Ott I, Metzler-Nolte N (2011) J Med Chem 54:3–25
23. Jaouen G, Vessièresab A, Top S (2015) Chem Soc Rev 44:8802–8817
24. Bruyère C, Mathieu V, Vessières A, Pigeon P, Top S, Jaouen G, Kiss R (2014) J Inorg Biochem 141:144–151
25. Patra M, Gasser G (2017) Nat Rev Chem 1:0066
26. Meier-Menches SM, Gerner C, Berger W, Hartinger CG, Keppler BK (2018) Chem Soc Rev 47:909–928
27. Lazic S, Kaspler P, Shi G, Monro S, Sainuddin T, Forward S, Kasimova K, Hennigar R, Mandel A, McFarland S, Lilge L (2017) Photochem Photobiol 93:1248–1258
28. Zamora A, Vigueras G, Rodríguez V, Santana MD, Ruiz J (2018) Coord Chem Rev 360:34–76
29. Lopresti AL (2018) Adv Nutr 9:41–50
30. Nelson KM, Dahlin JL, Bisson J, Graham J, Pauli GF, Walters MA (2017) J Med Chem 60:1620–1637
31. Musib D, Pal M, Raza MK, Roy M (2020) Dalton Trans 49:10786–10798
32. Ferrari E, Pignedoli F, Imbriano C, Marverti G, Basile V, Venturi E, Saladini M (2011) J Med Chem 54:8066–8077
33. Khatun B, Baishya P, Ramteke A, Maji TK (2020) New J Chem 44:4887–4897
34. Arezki A, Chabot GG, Quentin L, Scherman D, Jaouen G, Brulé E (2011) Med Chem Commun 2:190–195
35. Banerjee S, Chakravarty AR (2015) Acc Chem Res 48:2075–2083
36. Pröhl M, Schubert US, Weigand W, Gottschaldt M (2016) Coord Chem Rev 307:32–41
37. Wanninger S, Lorenz V, Subhan A, Edelmann FT (2015) Chem Soc Rev 44:4986–5002
38. Das D, Banaspati A, Das N, Bora B, Raza MK, Goswami TK (2019) Dalton Trans 48:12933–12942
39. Handler N, Jaeger W, Puschacher H, Leisser K, Erker T (2007) Chem Pharm Bull 55:64–71
40. Amouyal E, Homsi A, Chambron J-C, Sauvage J-P (1990) J Chem Soc Dalton Trans 1841–1845
41. SADABS, Bruker AXS Inc., Madison, Wisconsin, USA (2012).
42. Sheldrick GM (2015) Acta Cryst C 71:3–8
43. Mcghee JD, Hippel PHV (1974) J Mol Biol 86:469–489
44. Carter MT, Rodriguez M, Bard AJ (1989) J Am Chem Soc 111:8901–8911
45. Banaspati A, Das D, Choudhury CJ, Bhattacharyya A, Goswami TK (2019) J Inorg Biochem 191:60–68
46. Banaspati A, Raza MK, Goswami TK (2020) Eur J Med Chem 204:112632
47. Das D, Raza MK, Goswami TK (2020) Polyhedron 186:114614
48. Raza MK, Gautam S, Howlader P, Bhattacharyya A, Kondaiah P, Chakravarty AR (2018) Inorg Chem 57:14374–14385
49. Raza MK, Mitra K, Shettar A, Basu U, Kondaiah P, Chakravarty AR (2016) Dalton Trans 45:13234–13243
50. Upadhyay A, Gautam S, Ramu V, Kondaiah P, Chakravarty AR (2019) Dalton Trans 48:17556–17565
51. Mitra K, Gautam S, Kondaiah P, Chakravarty AR (2015) Angew Chemie-Int Ed 54:13989–13993
52. Dougan SJ, Habtemariam A, McHale SE, Parsons S, Sadler PJ (2008) PNAS 105:11628–11633
53. Romero-Canelón I, Mos M, Sadler PJ (2015) J Med Chem 58:7874–7880
54. Goswami TK, Gadadhar S, Roy M, Nethaji M, Karande AA, Chakravarty AR (2012) Organometallics 31:3010–3021
55. Goswami TK, Gadadhar S, Gole B, Karande AA, Chakravarty AR (2012) Eur J Med Chem 63:800–810
56. Maity B, Roy M, Banik B, Majumdar R, Dighe RR, Chakravarty AR (2010) Organometallics 29:3632–3641
57. Kellett A, Molphy Z, Slator C, McKee V, Farrell NP (2019) Chem Soc Rev 48:971–988
58. Zhang Y, Sun T, Jiang C (2018) Acta Pharm Sin B 8:34–50
59. İnci D, Aydın R, Vatan Ö, Sevgi T, Yılmaz D, Zorlu Y, Yerli Y, Çoşut B, Demirkan E, Çinkılıç N (2017) J Biol Inorg Chem 22:61–85
60. Ammar AA, Raveendran R, Gibson D, Nassar T, Benita S (2016) J Med Chem 59:9035–9046
61. Banerjee S, Prasad P, Hussain A, Khan I, Kondaiah P, Chakravarty AR (2012) Chem Commun 48:7702–7704
62. Delaey E, Van Larr F, De Vos D, Kamuhabwa A, Jacobs P, De Witte P (2000) J Photochem Photobiol B 55:27–36
63. Wu L, Yang L, Huang J, Zhang L, Weng X, Zhang X, Shen C, Zhou X, Zheng C (2009) Chem Biodivers 6:1066–1076
64. Sarkar T, Banerjee S, Hussain A (2015) RSC Adv 5:16641–16653
65. Mjos KD, Orvig C (2014) Chem Rev 114:4540–4563
66. Qin J-L, Shen W-Y, Chen Z-F, Zhao L-F, Qin Q-P, Yu Y-C, Liang H (2017) Sci Rep 7(46056):1–18
67. Abyar S, Khandar AA, Salehi R, Hosseini-Yazdi SA, Alizadeh E, Mahkam M, Jamalpoor A, White JM, Shojaei M, Aizpurua-olaizola O, Masereeuw R, Janssen MJ (2019) Sci Rep 9(14686):1–11

Authors and Affiliations

Dhananjay Das[1] · Aisha Noor[2] · Md Kausar Raza[3] · Tridib K. Goswami[1]

✉ Md Kausar Raza
kausarraza91@gmail.com

✉ Tridib K. Goswami
tridibgoswami05@gmail.com

[1] Department of Chemistry, Gauhati University, Guwahati 781014, Assam, India

[2] Department of Biotechnology, Jamia Millia Islamia, New Delhi 110025, India

[3] Department of Inorganic and Physical Chemistry, Indian Institute of Science, Bangalore 560012, India